J Mater Sci (2011) 46:5197–5207
DOI 10.1007/s10853-011-5456-1

Consolidation by electrical resistance sintering of Ti powder

J. M. Montes · J. A. Rodríguez · F. G. Cuevas · J. Cintas

Received: 4 November 2010 / Accepted: 9 March 2011 / Published online: 22 March 2011

Abstract In this study, commercially pure Ti powder was consolidated by the electrical resistance sintering (ERS) technique. This consolidation technique consists of the application of pressure (around 100 MPa) to a powder mass at the same time that the powder is heated by the passage of an electric current of high intensity (around 10 kA), low voltage (around 5 V) and a frequency of 50 Hz. Several current intensities and dwell times were tested during the consolidation process. The work includes a microstructural study of the most relevant characteristics of the compacts. Furthermore, the obtained compacts were mechanically characterised by the measurement of their hardness distribution and by an indirect tensile test. For all the compacts, the average hardness and the strength resulting from the indirect tensile test are empirically related to the global porosity of the compact and the electric energy supplied during the consolidation process. This energy is a function of the intensity of the electric current and the dwell time. These empirical relationships can be useful to select the best process conditions. The results were compared with values obtained for specimens prepared with the same powder by the conventional powder-metallurgy route of cold die pressing and furnace sintering.

J. M. Montes (✉) · J. A. Rodríguez · J. Cintas
Department of Mechanical and Materials Engineering, Escuela Técnica Superior de Ingeniería, Universidad de Sevilla, Camino de los Descubrimientos, s/n, 41092 Sevilla, Spain
e-mail: jmontes@us.es

F. G. Cuevas
Department of Chemistry and Materials Science, Escuela Técnica Superior de Ingeniería, Universidad de Huelva, Campus La Rábida, Carretera Palos, s/n, 21819 Palos de la Frontera, Spain

Introduction

The conventional powder-metallurgy (PM) route consists of cold pressing a powder mass to obtain a green compact, which is later furnace sintered to obtain the final consolidated specimen. Although this technology has a wide range of industrial uses, new alternatives are continuously under study. These new routes aspire to improve, at least partially, the problems and deficiencies of the current technology. In this sense, the direct use of electricity as a route for powder consolidation (especially with conductive powders) has been suggested and studied several times, generally from an experimental point of view. Several modalities and variants have been proposed that could be grouped under the generic name of "electrical sintering techniques". Recently, the designation of *Field-Assisted Sintering Techniques*, abbreviated as *FAST*, has become popular. It is true that speed is the most remarkable characteristic that all of these techniques have in common.

One of the FAST techniques, the so-called *Electrical Resistance Sintering* (ERS), was already described in 1933 by Taylor [1], although its systematic study was not carried out until some years later by Lenel [2], around 1955. Later, the ERS technique was the subject of numerous studies [3–14]. The ERS technique consists of applying an alternating electric current of low voltage and high intensity to a powder mass contained in an isolating die for a few seconds whilst, at the same time, pressure is applied. As the electric requirements (low voltage and high intensity) are perfectly satisfied by resistance welding equipment, one of such piece of equipment was the basis for the implementation of the ERS technique in this study.

The ERS technique was used in this study for the consolidation of commercially pure titanium (referred to as cp-Ti). The interest of this material [15–18] lies in its

excellent properties (especially its low density, high specific resistance and high corrosion resistance), which make it extraordinarily attractive for the aeronautic and aerospace industries, which demand half of the titanium produced. This complete dominance makes the price of the metal vary widely depending on the economical cycle of the aerospace industry, which makes difficult for Ti to penetrate traditional industries. The greatest challenge of the Ti industry is to gradually increase its market to reach that of the large series automotive industry. One of the necessary conditions to achieve this objective is the development of economic processing routes, where the PM will play a fundamental role during the next several years.

Despite these good omens, the conventional PM processing of Ti is, at this moment, riddled with obstacles. In particular, both the high reactivity of the Ti and the need for long sintering times require a sintering process under high vacuum conditions, which complicates and increases the price of the process. The use of sufficiently fast consolidation techniques, such as ERS, could make the use of controlled atmospheres unnecessary and would be a major step forward in the cost reduction of the process.

In this study, the hardness and indirect tensile strength of compacts prepared by the ERS of titanium powder were determined, and these values were compared with the same properties obtained with the conventional route. Furthermore, the study is accompanied by a microstructural analysis that highlights the differences between the electrical consolidation technique and the conventional route of cold pressing and furnace vacuum sintering.

Materials and experimental procedure

Cp-Ti powder, Ti 325 from Sejong Materials Co., was used in this research. Its more remarkable impurities are <0.045 wt% O and <0.08 wt% N (being nearly class 4, according to the ASTM standards [19]). A detailed chemical analysis as proportioned by the manufacturer is given in Table 1.

This powder has an irregular shape and a mean particle diameter of 24.2 μm (as determined by laser diffraction). Figure 1 shows a scanning electron microscopy (SEM) image of the powder particles and an optical micrograph of the internal microstructure of the powders (composed of α-Ti phase grains and without any other remarkable details).

Table 1 Chemical analysis of the Ti 325 powder as proportioned by Sejong Materials Co

	Ti	Fe	Si	O	N	Mg	Mn
Wt%	>99.5	0.038	0.035	<0.045	<0.08	0.003	0.0006

There is no commercial equipment available to carry out an electrical resistance sintering process. However, the electrical requirements—high intensity and low voltage—are appropriately satisfied by a resistance welding machine, which can also provide the necessary mechanical load for compression. A resistance welding machine (Serra Soldadura S.A., Spain) was adapted for this study. The machine consists of a monophase transformer of 100 kVA, a pneumatic cylinder capable of providing a uniaxial force of up to 14 kN, and an electronic controller that governs the sequences of the process to regulate the direct current intensity to a given value. Follow-up sensors of the outstanding parameters of the process were installed to record the displacement of the mobile punch, the applied load and the effective values of the voltage and current intensity.

The powder container die was made with an alumina pipe enclosed by a metallic hoop. The die had an orifice of 12 mm in diameter to host the powders. The die is closed on the top and bottom orifices with punches of temperature resistant copper (98.9%Cu–1%Cr–0.1%Zr). The powder mass to be sintered is located amongst those punches. Two wafers of the alloy 75.3%W–24.6%Cu (resistant to the electric erosion) are located in direct contact with the powder. They have the function, due to their small thermal conductivity, of dumping the flow of heat generated in the powder mass towards the water cooled electrodes (Fig. 2).

During the consolidation of the powder by ERS, the compaction pressure was fixed to 80 MPa. Several combinations of current intensity (from 3.5 to 6.0 kA) and current dwell time (from 40 to 80 cycles, with 1 cycle = 0.02 s) were tested; only one pulse was used to consolidate each specimen. During the process, the evolution of the electrical resistance of the specimens was calculated via the measurement of both the voltage between the electrodes and the intensity current. The variation of the porosity of the powder mass was determined through the knowledge of the punch displacement together with the measurement of the final porosity of the sintered compact.

Furthermore, to compare the ERS process with the conventional PM route, cylindrical compacts were also processed by the conventional route. These compacts were uniaxially cold pressed to attain a density of the 90% (1080 MPa according to the compressibility curve of the powder) and furnace sintered (1300°C, a high vacuum of 10 mPa and a sintering time of 150 min), according to conditions taken from the literature [20].

The sintered compacts, both electrically consolidated and processed via the conventional route, were tested to characterise (a) their hardness (*HV5*) distribution and the average hardness and (b) their indirect tensile strength.

Hardness tests were carried out after cutting the cylindrical compacts by the diametrical plane and mounting

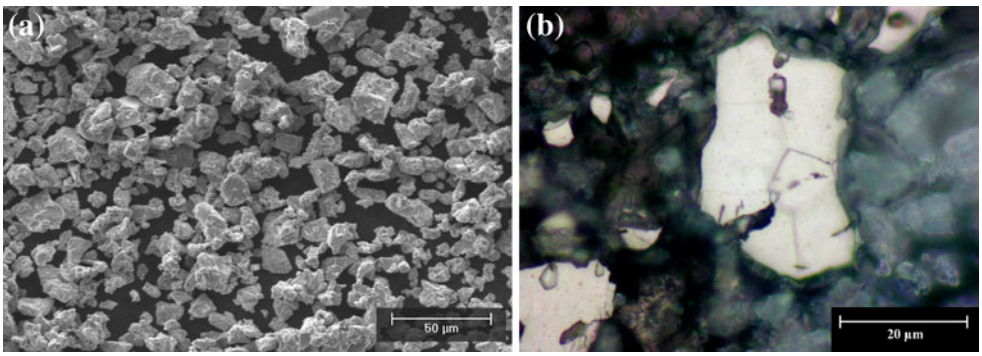

Fig. 1 **a** Scanning electron microscopy (SE-SEM) image of the cp-Ti powder and **b** optical micrograph of the cp-Ti powder etched with the Kroll agent

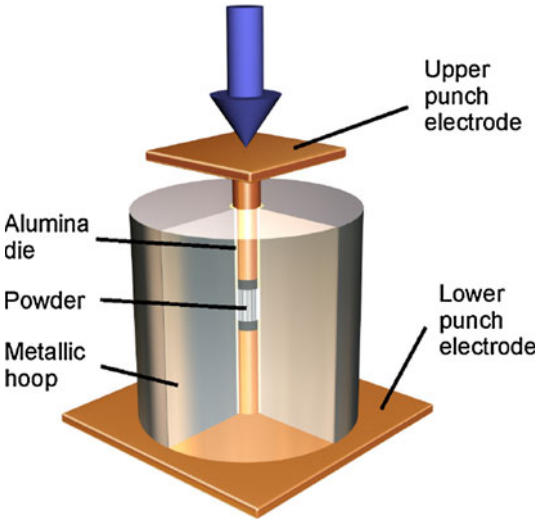

Fig. 2 Schematic representation of the different parts of the zone where the powders are sintered in the ERS experiments. The upper electrode is the only one with movement allowed

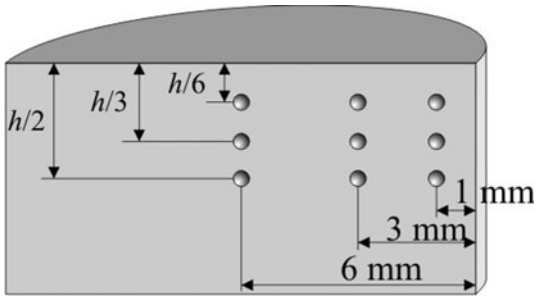

Fig. 3 Indentation map on a quadrant of a diametrical section for the determination of the hardness distribution. The hardness distribution in the other quadrants is supposed to be known due to the symmetry of the compact. The nine indicated indentations were used to determine the mean hardness of the specimens

them in Bakelite resin. For the ERS compacts, hardness test were constrained to only one quadrant, following a distribution such as the one shown in Fig. 3 (indentation in different places is needed in electrically consolidated compacts due to the nonuniform distribution of the porosity, which is a consequence of the temperature gradient generated in the compact during the consolidation process).

The indirect tensile tests are carried out by placing the cylindrical compacts on their lateral surface, not on their bases (Fig. 4a). They are then subjected to an increasing load until breaking (Fig. 4b). Once the breaking load of the compact (P_{max}) is found, the *Indirect Tensile Strength* (σ_{ITS}) can be estimated due to the fact that the vertical and diametrical plane of the cylindrical compact breaks with a tensile type fracture. The value of the σ_{ITS} can be calculated with

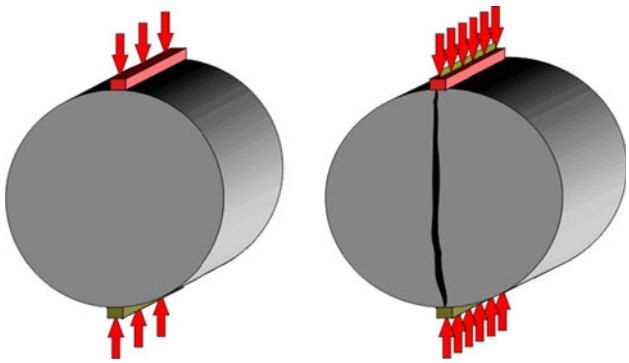

Fig. 4 Scheme of the operating arrangement in the indirect tensile test of the compacts

$$\sigma_{ITS} = \frac{P_{max}}{\pi r H} \quad (1)$$

where r is the compact radius and H its height.

In the case of ductile materials, the break will be not achieved, and the compact will be strongly deformed. In this situation, the test does not give any quantitative value. There is no specific standard for this test in the PM

field, and thus the conditions considered for the tests were taken from the literature [21].

Results and discussion

Chemical analysis

The clue for successful Ti processing is the control of the interstitials O, C and N. Therefore, chemical analysis of the starting powders and some of the various consolidated specimens were carried out (Table 2).

The N content measured for the starting powder is in the order of that given by the manufacturer (see Table 1), but for the O content now measured is almost the double. On the other hand, some differences appear after the sintering process. Thus, the C and N content increase to the double of the original content; however, the O content increases in a significant way.

Densification kinetics

Figure 5 shows the typical evolution of the global porosity and the electrical resistance of a powder mass processed by ERS. The curves are not parallel, and the decrease of the resistance curve is much more marked than that of the porosity curve.

The much different behaviour of the curves in Fig. 5 is due to the oxide layers surrounding the metallic powder particles. The dielectric or semiconductor nature of these layers provokes a strong dependence of the electric behaviour on the temperature. This dependence is exponential in such a way that a small increase of the temperature makes the resistivity quickly decay. Despite the small thickness of the dielectric layer, its resistivity governs the electric behaviour of the whole powder particle [22], and, when this resistivity drops, the resistivity of the compact decays. Also the self-getter effect of Ti, i.e. the dissolution of the oxide layers in the bulk material above a given temperature threshold, should be considered despite the shortness of the ERS process, as shown by the increase in the O content in the ERS processed specimens. This significant resistivity decrease occurs even before the temperature reaches sufficient values to provoke material softening. This softening, together to the continuously

Table 2 Chemical analysis (wt%) of the starting Ti 325 powder and a high-energy ERS consolidated specimen

	O	C	N
Ti 325 powder	<0.01	0.011	0.016
ERS consolidated Ti	0.42	0.025	0.033

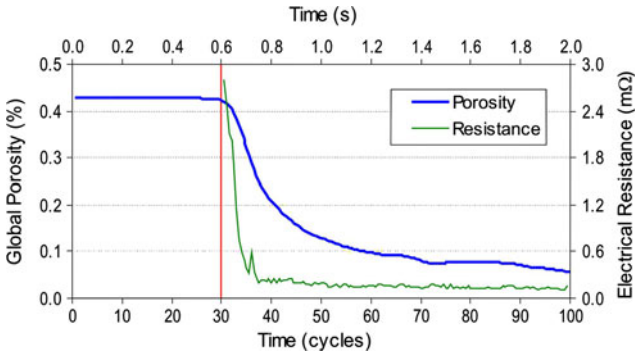

Fig. 5 Evolution of the porosity and the electrical resistance during a typical experiment of ERS. The vertical line ($t = 30$ cycles) points out the beginning of the passing of current. The end of the time scale ($t = 100$ cycles) indicates the end of the current passage but not of the pressure application, which is prolonged for 60 more cycles. The curves correspond to an experiment carried out with 4.5 kA for 70 cycles

applied pressure, is responsible for the material densification. During densification, the resistivity of the remaining dielectric layers decreases so much that the compact resistance is no longer governed by them. Only the increase of the metal–metal contacts and the increase of the area of the contacts associated with the porosity reduction cause the electric resistivity to decay, although, from then on, not in a significant way. Yet, such a decrease is partially compensated by the thermal increase of the metal resistivity, which reaches an approximately continuous resistance value during the process.

The *final porosity* Θ (i.e. the volumetric fraction of pores) of the ERS consolidated compacts, as a function of the current intensity (I) and the current passing time (t), is given in Table 3.

Table 3 indicates that the final porosities follow a reasonable trend (it would be expected for the porosities to decrease from top to bottom and from left to right) in most cases. Deviations are not uncommon in PM processes. It would be possible, in principle, to carry out bidimensional interpolations from the data shown in Table 3 to estimate, for given values of I and t, the value of the final porosity

Table 3 Values (expressed in %) of the compacts final porosities (Θ) for the different ERS experiments (1 cycle = 0.02 s)

		t (cycles)				
		40	50	60	70	80
I (kA)	3.5	18.00	17.26	16.59	15.26	13.81
	4.0	15.49	15.79	15.17	14.68	13.49
	4.5	13.42	13.45	11.89	10.17	9.60
	5.0	9.88	9.36	7.49	7.77	7.62
	5.5	8.07	8.05	7.36	6.15	5.89
	6.0	6.79	4.89	4.36	3.34	3.26

(Θ) of the compact. However, a new magnitude, more suitable than I and t, can be considered for an appropriate description of the process: the *thermal energy generated by the Joule effect*.

Specific thermal energy (η)

The parameter η is the *thermal energy generated per unit mass* of the powder (*specific thermal energy*) due to the Joule effect. Table 4 shows the values of η corresponding to the different combinations of intensity and dwell time in the ERS experiments. These values were calculated by time integration of the curve of the dissipated electrical power in the powder aggregate (and transformed to thermal energy) during the consolidation process; that is,

$$\eta = \frac{1}{M}\int_0^t I^2 R(\tau)\mathrm{d}\tau \qquad (2)$$

where I is the current intensity crossing the powder aggregate, R is the electrical resistance of the powder aggregate (obtained from curves such as that of Fig. 5) and M is the powder mass. The integration shown in Eq. 2 was computed by a numerical method. As expected, the values of η in Table 4 grow from top to bottom and from left to right.

Table 4 Values of η (expressed in kJ/g) for the different ERS experiments (1 cycle = 0.02 s)

		t (cycles)				
		40	50	60	70	80
I (kA)	3.5	1.09	1.30	1.43	1.67	1.77
	4.0	1.27	1.45	1.62	1.88	2.11
	4.5	1.43	1.78	2.05	2.30	2.58
	5.0	1.69	1.96	2.35	2.62	2.99
	5.5	1.88	2.35	2.72	2.96	3.46
	6.0	2.08	2.57	2.97	3.31	3.72

Curves Θ versus η

The final porosity, Θ, is plotted in Fig. 6 versus the calculated values of the specific thermal energy (η). Figure 6a, b only differs in how the dots are classified: (a) by identical dwell time and (b) by identical current intensity in the ERS experiments. The linear trend line appearing in the figures was obtained by the least squares method.

As expected, higher values of η (i.e. higher intensities and current passing times) cause the porosity to reach a minimum value, which is about 3.3% for the conditions tested. A quick view of the graphs in Fig. 6 shows that conclusions cannot be easily drawn when the intensity or time are considered separately. For instance, without Fig. 6b, it could be thought that all the experiments at 3.5 kA are less energetic that those carried out at 4.0 kA. However, the experiment at 3.5 kA and 70 cycles is more energetic that the experiment at 4 kA and 50 cycles, which is not easy to predict a priori because the electrical resistance of the compact is unknown. The magnitude of η helps to overcome this inconvenience.

Metallographic study

The marked differences between the ERS and conventional processing are translated into significant microstructural differences in the compacts obtained by both methods. Figure 7 shows three macrographs of diametrical sections of three cylindrical compacts, the first one (Fig. 7a) consolidated by the conventional PM route and the other two (Fig. 7b, c) consolidated via ERS (4.0 kA and 50 cycles, and 6.0 kA and 80 cycles, respectively).

The porosity distribution of these compacts is quite different. For the conventionally consolidated compacts, the distribution is relatively uniform; however, the ERS consolidated compacts show a nonuniform distribution characterised by a perimeter that is more porous than the centre, which is much more visible in the low η compact. This nonuniform distribution of the porosity is a consequence of the inhomogeneous distribution of the temperature during the sintering process, where the temperature is

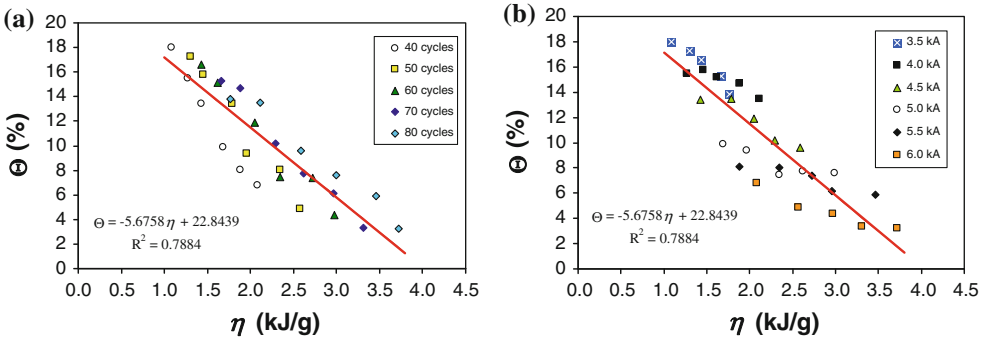

Fig. 6 Final porosity (Θ) of electrically sintered compacts as a function of the specific thermal energy (η). Values are grouped by **a** families of equal dwell time, and **b** families of equal current intensity

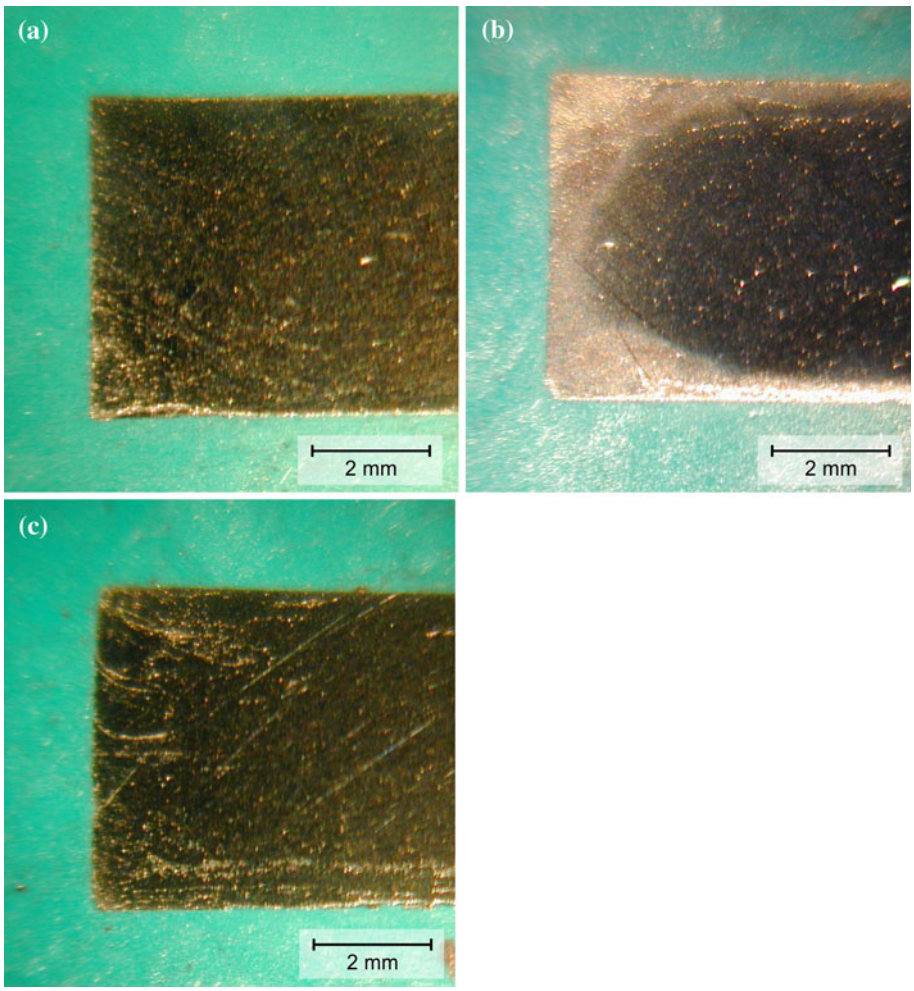

Fig. 7 Macrographs of diametrical sections of half of **a** a compact that was conventionally sintered (with a porosity of 2%), **b** an electrically consolidated compact (4.0 kA, 50 cycles, and a porosity of 15.8%), and **c** another electrically consolidated compact (6.0 kA, 80 cycles, and a porosity of 3.3%). The ERS compact consolidated with low η shows a kind of aureole due to a high porosity area near the periphery. The high-η ERS compact shows a more uniform porosity than the one with low η and a porosity level higher than the conventionally consolidated compact

higher in the compact centre and lower towards the bases and the lateral walls, as already observed by Lenel [2] in experiments carried out with several metals. The temperature decrease near the bases is due to the cooling provoked by the refrigerated electrodes. In contrast, the lateral temperature decrease is caused by the contact of the compacts with the die walls, initially at room temperature and with a lower thermal conductivity.

Another factor that can contribute to the porosity heterogeneity in ERS compacts is the evacuation of gases during heating. As a consequence of the speed of the process and the simultaneous compacting and heating processes, pores can close when gasses remain in the compact, causing some residual porosity. However, during the conventional processing, the slow heating process, the use of a vacuum atmosphere and the usual presence of open porosity in the green compact decrease the probability of pores closing.

A detailed study of the pore morphology of ERS compacts can differentiate three types of pores (Fig. 8). The first one consists of a porosity that is localised in an easily visible aureole in the compact borders (Figs. 7b, 8a). These pores are in regions of abundant porosity, showing an irregular shape and a size comparable to the powder particles size, which is a consequence of a deficient sintering process. A second type of porosity is uniformly distributed over the whole compact (Fig. 8b). This residual porosity is present even when the compact is well sintered. It consists of small and rounded pores (with a diameter of around 3 μm), representing a very small fraction of the total volume of the compact. Finally, the third type of porosity is only observed in compacts processed with high current intensity and consists of isolated and planed large pores, with the greater axis perpendicular to the punch axis but with some inclination due to the punch movement (Fig. 8c). Yet, it should be considered that these pores could really not be pores but shear cracks introduced during pressing, probably as a consequence of friction between the punch faces and the compact. These pores appear in lines and only near the upper punch, which is the only one with movement allowed.

Concerning the phases present in the material and given that it is a commercially pure Ti, the two possible phases

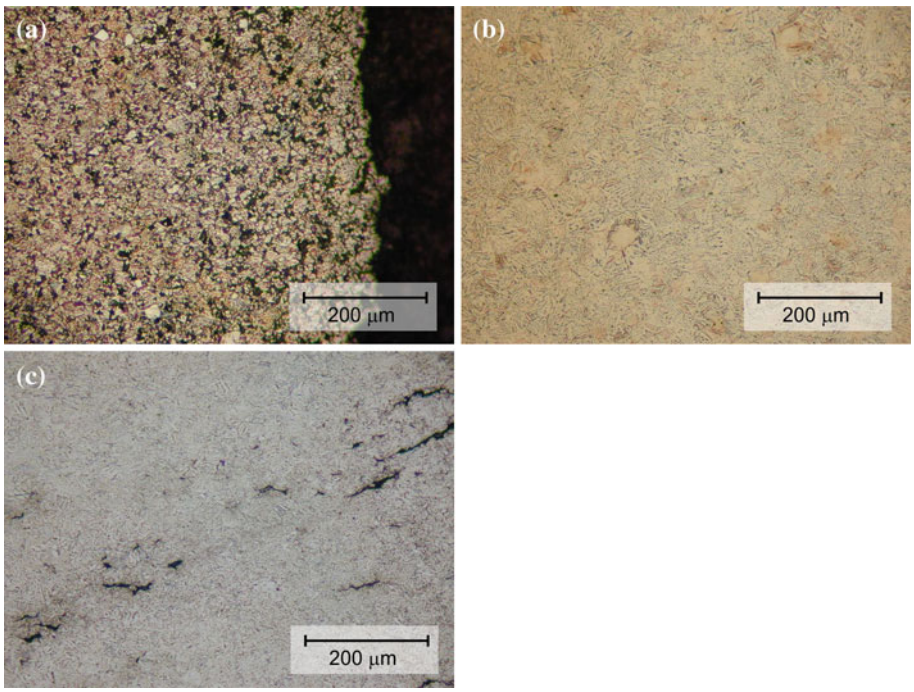

Fig. 8 Micrographs of the different types of pores found in ERS compacts: **a** large pores in the compact perimeter, **b** almost invisible small pores and **c** isolated and planed large pores

are the allotropic varieties of Ti, i.e. α-Ti (hcp structure) and β-Ti (bcc structure). The microstructure of the initial powder, as shown in Fig. 1b, consists of only α-Ti grains with an equiaxial morphology.

Considering the composition of the Ti Sejong (which is nearly class 4), its β-transus temperature (the transformation temperature from α–β phase, or all-α phase, to all β) is about 920°C. Under a slow enough cooling from the β zone, as the furnace cooling from 1300°C corresponding to the conventional route, a large-grain, irregular and equiaxed morphology is developed in the secondary α grains (Fig. 9a). The new grains, similar in shape to those of the original powders, now have a size of about 200 μm versus the 12 μm of the original powders. In contrast, when analysed at a high enough magnification by EDX-SEM, the rest of the β phase (the dark area in Fig. 9b) is still present, as well as a few grains with Ti–Fe needles due to some impurities in the powder composition.

Lamellar α morphology is the most common phase appearing from the β phase transformation during faster cooling as a result of a nucleation and growth process on crystallographic planes of the β matrix. This growth process usually occurs on multiple orientations of the planes family, with the lamellas grouped in clusters or colonies aligned in the same orientation. It is the most remarkable microstructure of the electrically consolidated compacts (Fig. 10a), with larger lamellar grains at higher values of η. In the case of low η, colonies uniformly distributed in the inner of the compact appear, where the lamellar structure is clearly developed. However, most of the compact consists

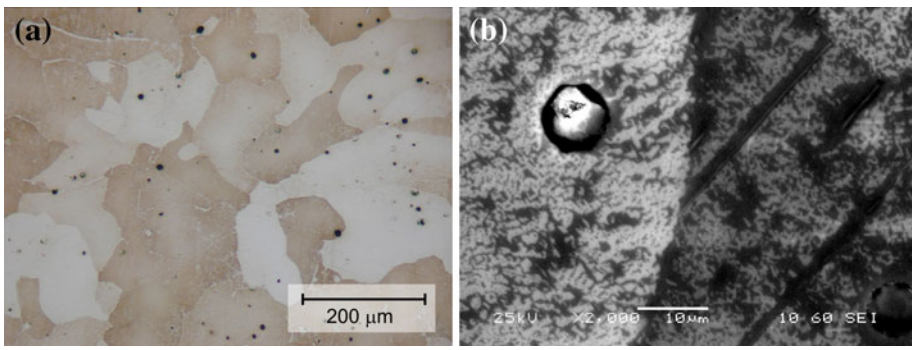

Fig. 9 **a** Optical micrograph of a compact (porosity of 1.5%) consolidated via the conventional PM route (etched with HF 0.5%) with a microstructure predominantly consisting of equiaxed α grains and some residual porosity typical of PM products. **b** SE-SEM micrograph where a pore, a grain boundary, α and β phases, and Ti–Fe needles are observed

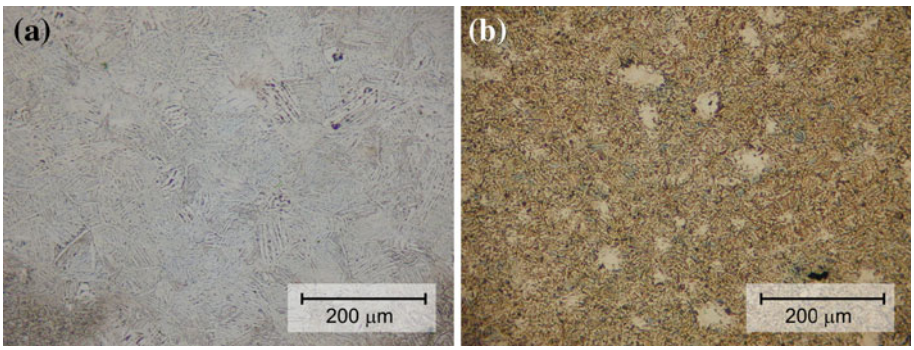

Fig. 10 Optical micrographs of **a** the lamellar structure appearing in ERS compacts (in this case consolidated with 6.0 kA and 80 cycles, porosity 3.26%) and **b** the mixture of colonies with lamellar structure and a matrix where the lamellar structure is not totally developed (compact consolidated with 4.0 kA and 50 cycles, porosity 15.79%)

of grains where the β structure is retained together with small lamellas of α phase (Fig. 10b).

Still, near the compacts limits, equiaxed α grains are observed (Fig. 11). Two factors, probably acting together, might be the cause of this microstructure: the lower temperature reached, which does not permit the appearance of the β phase and its transformation to secondary α, and the absorption of oxygen and nitrogen from the air at the reached temperature, or from the powder itself, which stabilises a hard and brittle α phase known as α case. The porosity in these areas is much higher, especially for low η, with pores of similar size to the particle size (Fig. 11a). This porosity appears in big, aligned, and planed pores for high η (Fig. 11b).

In summary, Fig. 12 shows different micrographs from regions at several distances from the centre of a diametrical section of an ERS consolidated compact. The different images show the variation of the lamellar microstructure, which is finer farther from the centre (due to the lower temperature and grain growth) and nearer to the die walls. A high porosity can also be observed in the compact borders.

The aforementioned microstructure very much affects the mechanical properties in different zones of the compact. For instance, the outer layer of low-η compacts, with a high porosity and a microstructure consisting in brittle α grains (hcp structure), would probably have to be removed before use. Fortunately, to reduce the porosity and the thickness of the outer layer, it is sufficient to consolidate under high-η conditions.

Vickers hardness

It is expected that the compacts with a higher level of densification show a greater hardness, but it is necessary to clarify this idea because hardness is not uniformly distributed in the compact. The central zone normally has the highest value of the hardness. This heterogeneity in the hardness distribution and in the porosity is a consequence of the heterogeneous temperature distribution during the process, which is characteristic of the ERS technique. The temperature reached in the central zone helps the diffusion process, and, therefore, both the size and the number of pores diminish (as corroborated by metallographic analysis). Hardness measurements performed according to the pattern shown in Fig. 3 reveal that the central value can be up to 2.5 times the hardness measured in the lateral of the compact. Nevertheless, increasing the η value (more energetic experiences) causes the higher hardness point to be located away from the compact centre, at symmetrical points on the vertical. This effect can be due to an excessive heating of the central zone, which causes hardness stagnation as a consequence of the grain coarsening. Table 5 shows the hardness distribution obtained in two representative compacts prepared in experiences with different η values.

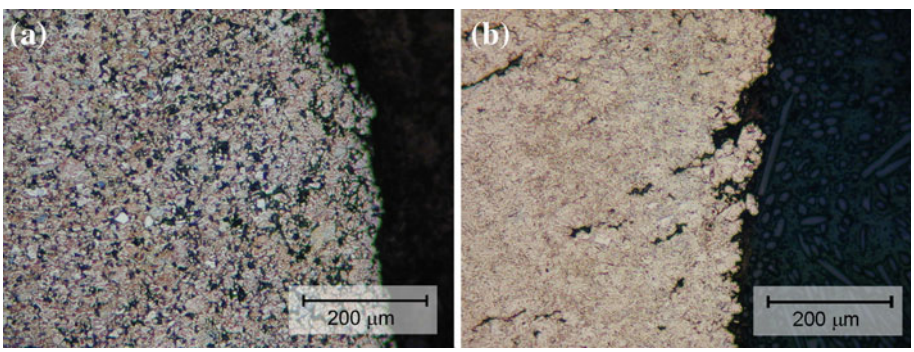

Fig. 11 Peripheral zone of ERS compacts with equiaxed α grains in **a** a compact consolidated with low η (4.0 kA and 50 cycles, porosity 15.79%) and **b** a compact consolidated with high η (6.0 kA and 80 cycles, porosity 3.26%)

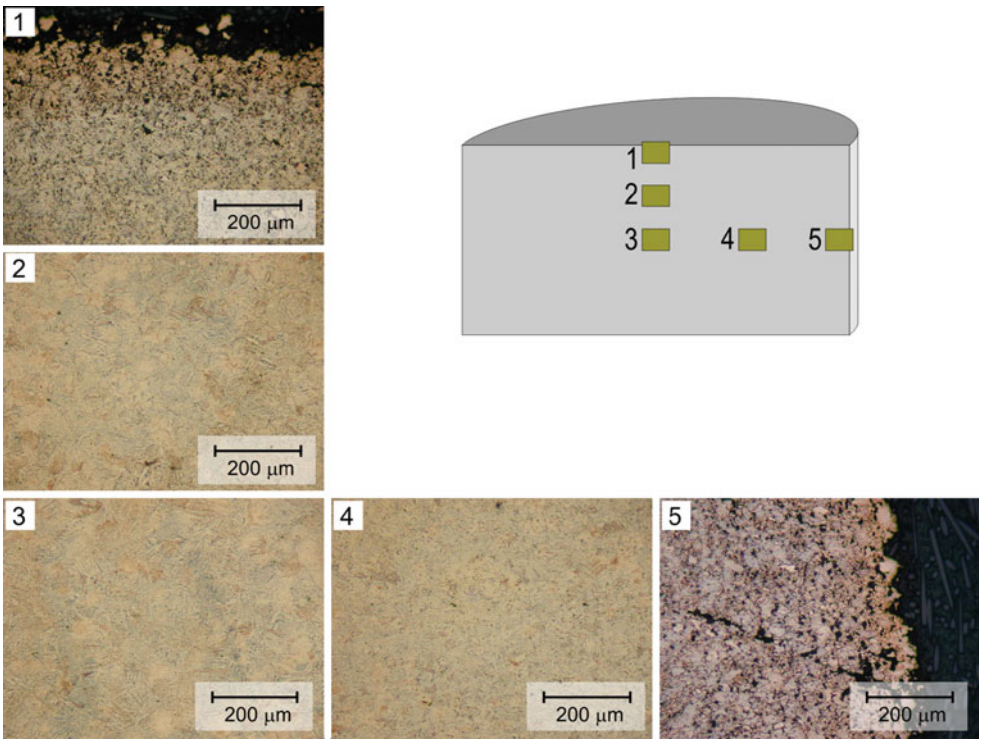

Fig. 12 Microstructure and porosity distribution on a diametrical section of a cp-Ti compact consolidated via ERS with 4.5 kA and 70 cycles (porosity 10.17%)

Table 5 Hardness distribution, in the nine indentations indicated in Fig. 3, on two ERS specimens

$\eta = 1.09$ kJ/g (3.5 kA and 40 cycles)		
176	176	109
218	217	106
227	230	104
$HV5 = 174 \pm 54$		
$\eta = 2.96$ kJ/g (5.5 kA and 70 cycles)		
399	389	212
434	428	316
373	390	380
$HV5 = 369 \pm 68$		

HV5 represents the mean value with its standard deviation

To obtain more general conclusions, Fig. 13a plots the mean hardness, *HV5* versus η. The mean hardness is calculated as the average of the hardness values measured in the set of dots distributed on a diametrical section of the cylindrical compact (Fig. 3). Figure 13b plots the mean hardness versus the porosity. In both cases, there is a linear dependence, although this is much clearer in the case of *HV5* versus Θ (the mean hardness is inversely proportional to the porosity level of the compact).

Still, it is remarkable that the hardness attained via the ERS process is, in general, lower than that achieved by the conventional route (around 440 *HV5*). Only in the most energetic experiments (higher values of η) are the hardness mean values of the same order as those of the conventional compacts, which is a logical result because the most energetic ERS experiments obtain better joining amongst the powder particles, which is translated as a hardness increase.

It is also remarkable in Fig. 13 that, for the more energetic experiments, the hardness seems to start to decay, which could be due, as aforementioned, to the progressive increase in the grain size. However, due to the high data scattering, a linear trend was established, ignoring this factor.

Indirect tensile test

The *indirect tensile strength* (σ_{ITS}) is plotted versus η and Θ in Fig. 14a, b, respectively. The behaviour shown in both graphs indicates that σ_{ITS} improves as η increases or the porosity decreases (this is, as the relative density increases). Both factors lead to a better joining between powder particles, the most important feature to obtain good tensile strengths in PM processed compacts (the respective fitting relationships show that the scattering is quite high in these cases).

The σ_{ITS} values for electrically processed compacts are lower than those achieved with the conventional process (around 290 MPa). Only in high η experiments do the σ_{ITS} values of the electrical compacts approach that level. This difference is a consequence of the extraordinarily short duration of the ERS process. A later annealing of the electrically sintered compact might improve the tensile strength but might also cause a loss of hardness.

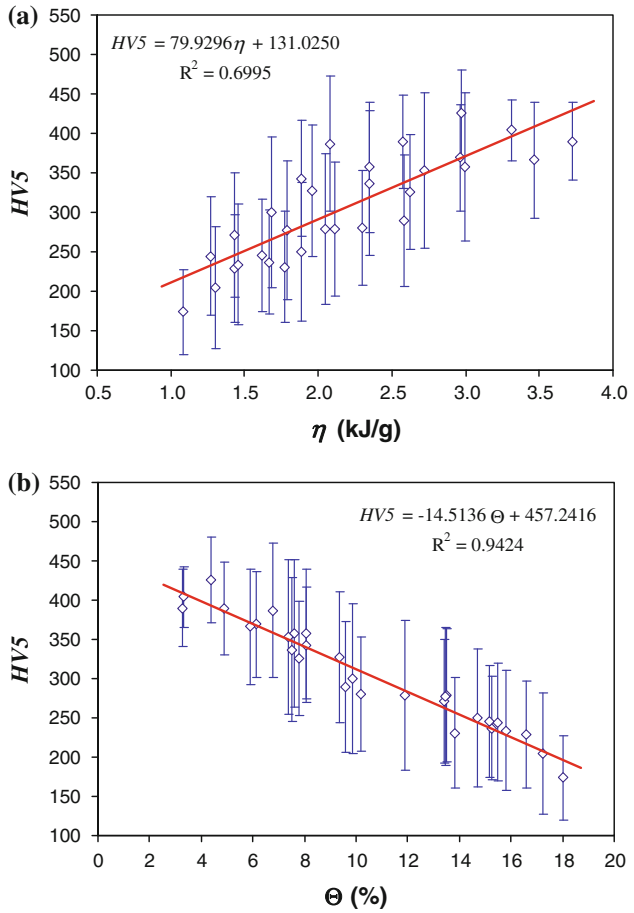

Fig. 13 Mean hardness (*HV5*) versus **a** specific thermal energy (η) and **b** final porosity (Θ), as measured in compacts sintered by the ERS technique

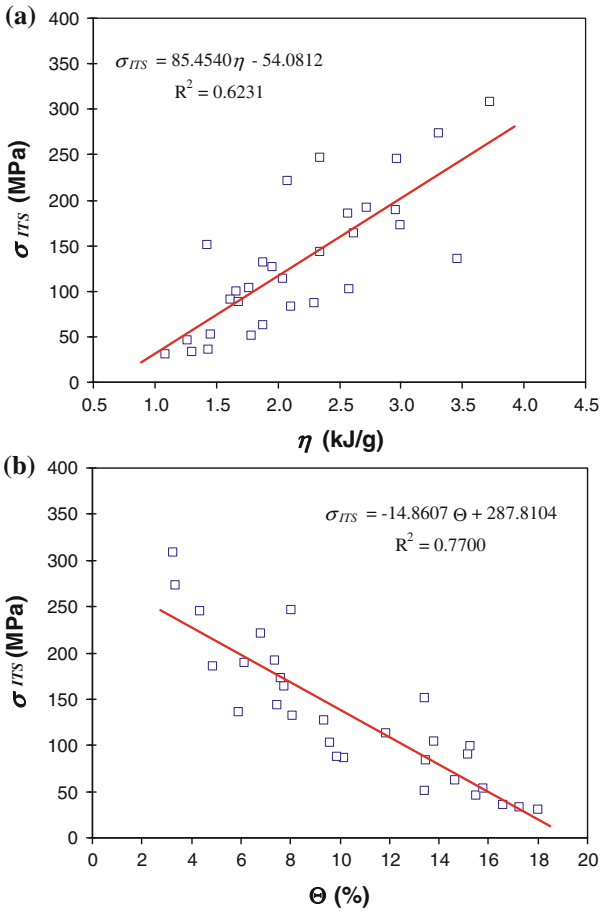

Fig. 14 σ_{ITS} versus **a** specific thermal energy (η) and **b** final porosity (Θ) as measured in compacts sintered by the ERS technique

A detail of the appearance of some of the ERS tested specimens is shown in Fig. 15.

Conclusions

Samples of cp-Ti were obtained via an ERS consolidation process at different current intensities (in the range 3.5–6.0 kA) and different dwell times (in the range 40–80 cycles). With this technique, it was possible to achieve final porosities of about 3.3, versus 1.5% that can be reached via the conventional route, but using pressures almost 14 times lower than those used in the conventional route (80 MPa vs. 1080 MPa) and much shorter consolidation times. Lower porosities are achieved when the intensity current and the dwell time are greatest, this is, when the *specific thermal energy* (η) is at a maximum.

The microstructural study revealed that the porosity is not uniformly distributed in the compacts consolidated via the ERS process, contrary to the observations of compacts consolidated via the conventional PM process of cold pressing and furnace vacuum sintering. The most characteristic porosity distribution in the ERS consolidated compacts consists of a very dense nucleus and a more porous periphery. The transition zone between both regions is observed as a kind of aureole, which the metallographic study revealed to be formed by abundant porosity. Another important difference with respect to the conventional technique is that the lamellar structure is always present in the ERS consolidated compacts. The presence of this microstructure, composed of thin laminas appearing in coherent groups, is a consequence of the high cooling rate of the ERS consolidated compacts.

However, the highest mean hardness was not achieved in the more energetic experiments. In this case, a decrease in the hardness of the compact core was observed due to excessive heating, which leads to grain coarsening of the bulk material. Thus, the hardness in the centre of the compact is not representative of the whole compact; it is necessary to consider the average hardness measured in a set of distributed indentations.

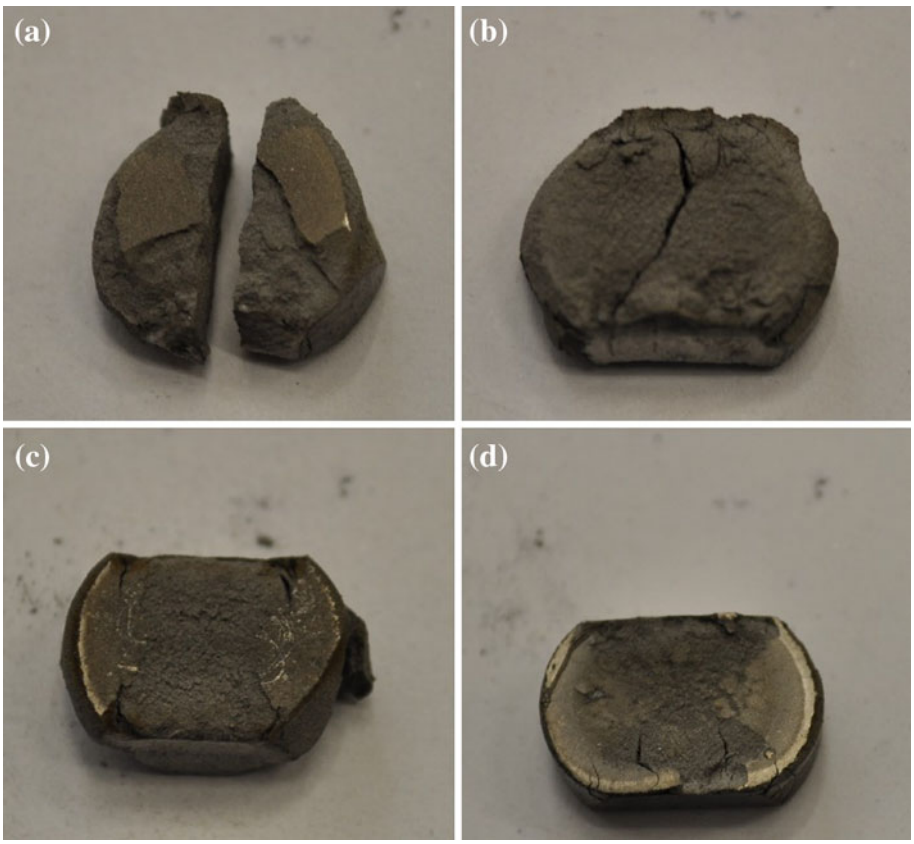

Fig. 15 Detail of some of the ERS specimens after the indirect tensile test; **a** 3.5 kA and 50 cycles (17.26% porosity), **b** 4 kA and 50 cycles (15.79% porosity), **c** 4.5 kA and 80 cycles (9.60% porosity), and **d** 6 kA and 50 cycles (3.26% porosity). It can be observed that the ductility of these materials is low, mainly for lower values of η

The indirect tensile strength clearly shows a decreasing trend as the porosity increases, which is logical because the pores can be the beginning of crack formation. In addition, lower porosities lead to a better joining between particles.

Acknowledgements The authors are grateful to FEDER/MCyT, Madrid, and Junta de Andalucía for funding this research within the framework of the Projects MAT2007-61643 and P08-TEP-3537, respectively. The authors also wish to thank the technicians J. Pinto, M. Madrid and M. Sánchez (Univ. Seville, Spain) for experimental assistance.

References

1. Taylor GF (1933) Apparatus for making hard metal compositions. US Patent 1896854, Feb 1933
2. Lenel FV (1955) J Met 7:158
3. Suzuki T, Saito S (1971) J Jpn Soc Powder Powder Metall 18:28
4. Saito S, Ishitama T, Sawaoka A (1974) Bull Tokyo Inst Technol 120:137
5. Hara Z, Akechi K (1980) In: Kimura H, Izumi O (eds) Titanium '80. Science and technology, proceedings of the 4th international conference on Ti, Kyoto, Japan, 19–22 May 1980. The Metallurgical Society of AIME, New York, p 2265
6. Okazaki K (1994) Rev Part Mater 2:215
7. Istomina TI, Baidenko AA, Raichenko AI, Golberg MA, Svechkov AV (1983) Sov Powder Metall Met Ceram 22(11):957
8. Burenkov GL, Raichenko AI, Suraeva M (1987) Sov Powder Metall Met Ceram 26(9):709
9. Sukhov OV, Baidenko AA, Istomina TI, Raichenko AI, Popov VP, Svechkov AV, Golberg MA (1987) Sov Powder Metall Met Ceram 26(7):530
10. Yokota M, Nagae T, Nose M (1998) Proceedings of the world congress PM'98, Granada, Spain, 18–22 Oct 1998. EPMA, Bellstone, Shrewsbury, p 284
11. Moriguchi H, Tsuduki K, Ikegaya A (2000) Powder Metall 43(1):17
12. Groza JR, Zavaliangos A (2000) Mater Sci Eng A 287:171
13. Montes JM, Rodríguez JA, Herrera EJ (2003) Rev Met Madrid 39:99 (in Spanish)
14. Montes JM, Cintas J, Cuevas FG, Rodríguez JA (2004) Proceedings of Euro PM 2004, Vienna, Austria, 17–21 Oct 2004, vol 2. EPMA, Bellstone, Shrewsbury p 259
15. Henriques VAR, Galvani ET, Petroni SLG, Paula MSM, Lemos TG (2010) J Mater Sci 45(21):5844. doi:10.1007/s10853-010-4660-8
16. Mao ZP, Ma J, Wang J, Sun B (2009) J Mater Sci 44(12):3265. doi:10.1007/s10853-009-3438-3
17. Tuncer N, Arslan G (2009) J Mater Sci 44(6):1477. doi:10.1007/s10853-008-3167-z
18. Li H, Yuan B, Gao Y, Chung CY, Zhu M (2009) J Mater Sci 44(3):875. doi:10.1007/s10853-008-3193-x
19. ASTM B 265-06a (2006) Standard specification for titanium and titanium alloy strip, sheet and plate. ASTM International, West Conshohocken, PA, USA
20. ASM Handbook (1998) Metal powder technologies and applications, vol 7. ASM International, USA
21. Capua JR, Michot G (2006) Int J Fract 139:455
22. Montes JM, Cuevas FG, Cintas J (2007) Metall Mater Trans B 38:957